J Therm Anal Calorim (2013) 113:843–847
DOI 10.1007/s10973-012-2830-4

Effect of the thermal treatment conditions on the formation of zinc ferrite nanocomposite, $ZnFe_2O_4$, by sol–gel method

Mohammad Hossein Habibi · Amir Hossein Habibi

Received: 9 September 2012 / Accepted: 16 November 2012 / Published online: 11 December 2012

Abstract Zinc ferrite nanocomposite was synthesized via thermal decomposition of zinc acetate and iron nitrate at three different temperatures (350, 450, and 550 °C). The influence of the thermal decomposition of precursors on the formation zinc ferrites was studied by differential thermal gravimetry and thermogravimetry (TG). The TG curve shows two steps for the thermal decomposition with mass loss of 17.3 % at 78 °C and 63.3 % at 315 °C. The prepared zinc ferrites nanocomposite was characterized by X-ray diffraction and scanning electron microscopy. The X-ray diffractograms of $ZnFe_2O_4$ shows that a crystalline phase, spinel system is formed. SEM micrograph of the zinc ferrite nanocomposite indicates the formation of uniformly spherical 48-nm nanograins. The properties of the zinc ferrite phase were strongly dependent on their calcinations temperature and molar ratio of precursors.

Keyword Zinc ferrite · Thermal decomposition · Iron precursor · Thermal properties · Nanostructure

Introduction

Nanocomposite magnetic materials are of great technological importance due to their distinctive chemical and physical properties [1–4]. The ferrite material is a widely studied class of magnetic materials with remarkable magnetic and electric properties having many of applications as components of electronic devices, magnetic fluids, medical diagnostics, and humidity sensors [5–9]. Zinc oxide is an important direct and wide bandgap semiconductor material (3.37 eV) with unique optical, acoustic, and electronic properties. Zinc oxide is well known with its high transparency and it has been applied in electronic and optoelectronic devices. Zinc oxide is non-toxic, possessing a high luminous transmittance, good electrical properties, and excellent piezoelectric properties. ZnO have been prepared by various techniques, among which, sol–gel technology is of perspective and low cost [10–21]. Ferrites, including zinc ferrite, are among the most significant magnetic materials due to vital application in information storage, electronic devices, magnetic resonance imaging, and drug delivery technology [1, 2, 22–24]. Synthesis of composite materials with fine nanostructures and excellent optical and magnetic properties is still a challenging topic [25–27]. The aim of this paper is to report preparation of a series of zinc ferrite nanocomposites and study the effect of thermal treatment conditions on the formation of zinc ferrite by sol–gel method.

In this research, we report the preparation of zinc ferrite, $ZnFe_2O_4$ nanocomposite by a simple sol–gel method. Thermal and spectral analyses were used for materials characterization. The effect of the zinc and iron precursor stoichiometric ratio on thermal decomposition process was studied by differential thermal gravimetry (DTG) and thermogravimetry (TG). The phase, morphology, particle diameter of samples, and optical properties were studied by X-ray diffraction (XRD), scanning electron microscopy (SEM), fourier transform infrared (FTIR), and UV–Vis diffuse reflectance (DRS) spectroscopy.

M. H. Habibi (✉) · A. H. Habibi
Nanotechnology Laboratory, Department of Chemistry, University of Isfahan, 81746-73441 Isfahan, Islamic Republic of Iran
e-mail: habibi@chem.ui.ac.ir

Experimental

Materials

Commercial compounds (Sigma-Aldrich, Merck), iron(III) nitrate, $Fe(NO_3)_3{\cdot}9H_2O$ (98 %), zinc acetate dihydrate $Zn(C_2H_3O_2)_2{\cdot}2H_2O$ (99.0 %), isopropyl alcohol (IP), monoethanolamine (MEA) were used as starting materials for synthesis of zinc ferrite nanocomposite.

Preparation of zinc sol and pure zinc oxide nanoparticle

Zinc acetate monohydrate, $Zn(C_2H_3O_2)_2{\cdot}H_2O$, 3.1 g as precursor was dissolved in the mixture of isopropyl alcohol, 15 mL as a solvent, and monoethanolamine, 0.86 mL as a complexing agent while stirring at 60 °C for 1 h and aged for 2 days to achieve a transparent zinc sol. The sol was dried at 110 °C. The powder was thermally treated by a gradual increase of temperature up to 300 °C. The powder was heat treated in air at 350, 550 °C for 4 h.

Preparation of iron sol and pure iron oxide nanoparticle

Iron nitrate nonahydrate, $Fe(NO_3)_3{\cdot}9H_2O$ 2.45 g as precursor was dissolved in the mixture of isopropyl alcohol, 15 mL as a solvent, and monoethanolamine, 0.86 mL as a complexing agent while stirring at 60 °C for 1 h and aged for 2 days to achieve a transparent iron sol. The sol was dried at 110 °C and the powder was thermally treated by a gradual increase of temperature up to 300 °C. The powder was heat treated in air at 350, 550 °C for 4 h.

Preparation of zinc ferrite sol and $ZnFe_2O_4$ nanocomposite

Iron nitrate nonahydrate, $Fe(NO_3)_3{\cdot}9H_2O$, 2.45 g powder added into zinc sol (zinc acetate monohydrate, $Zn(C_2H_3O_2)_2{\cdot}H_2O$, 3.1 g as precursor was dissolved in the mixture of isopropyl alcohol, 15 mL as a solvent, and monoethanolamine, 0.86 mL) with vigorous stirring to obtain a uniform sol. The sol was aged for 2 h at ambient temperature in a closed vessel. The mixtures of zinc sol and iron sol with molar ratios, 1:1, 1:2, 1.5:1, and 2:1 were prepared by mixing the solutions and drying in vacuum at 110 °C. The produced powder was thermally treated by a gradual increase of temperature up to 300 °C. The produced solids were thermally treated in air at 350, 450, and 550 °C for 4 h.

Characterization of nanocomposite

The XRD patterns of pure zinc oxide nanoparticle, pure iron oxide nanoparticle, and zinc ferrite nanocomposite were obtained using a Bruker D8 advance X-ray diffractometer using the Cu Kα ($\lambda = 1.5406$ Å) radiation with a scanning speed of 1° per min, 35 kV and 30 mA, the scanning in 2θ was from 2 to 70°. The thermoanalytical measurements (TG-DTG) study for the thermal decomposition of precursors were carried out using a Mettler TA4000 system from 20 to 700 °C at a heating rate of 5 °C min^{-1}. The morphologies and particle sizes of pure zinc oxide nanoparticle, pure iron oxide nanoparticle, and zinc ferrite nanocomposite were observed using FESEM (Hitachi, model S-4160) and Philips XL-30 scanning electron microscopy (SEM). UV-DRS spectra were recorded on a V-670, JASCO spectrophotometer. FT-IR absorption spectra of selected samples before and after heat treatment were obtained using KBr disks on a FT-IR 6300 in the region 4000–400 cm^{-1}.

Results and discussion

Figure 1 shows the TG and DTG curves for the pyrolysis of zinc acetate monohydrate using as precursor of zinc ferrite. The TG curve shows two steps for the thermal decomposition. The first step corresponds to the evolution of water of crystallization, reaching a constant mass loss of 17.3 % at 78 °C. The second step corresponds to the complete decomposition of zinc acetate monohydrate to ZnO reaching a constant mass loss of 63.3 % at 315 °C. The X-ray diffractograms of pure zinc oxide thermal decomposed at 550 °C (Fig. 2) shows that a crystalline ZnO phase (hexagonal system) [28]. Crystallite size of the pure ZnO phase was calculated by Scherrer's equation and they were within a narrow range of 17–23 nm which is comparable to SEM results (Fig. 3). The pattern intensities increased on increasing the calcination temperature from 350 to 550 °C. It can be seen that the crystalline zinc oxide phase may be formed at 550 °C (Fig. 2), as a result of a solid-state reaction between the corresponding oxides produced from the thermal decomposition of the starting materials zinc acetate monohydrate [29]:

$$Zn(C_2H_3O_2)_2{\cdot}\ H_2O \xrightarrow{78^{\circ}C} Zn(C_2H_3O_2)_2 + H_2O$$

$$Zn(C_2H_3O_2)_2 \longrightarrow Zn(C_2H_3O_2)(OH) + CH_3COOH$$

$$Zn(C_2H_3O_2)(OH) \longrightarrow Zn(OH)_2 + CH_3COOH$$

$$Zn(OH)_2 \xrightarrow{315^{\circ}C} ZnO$$

The TG–DTG curves of iron nitrate nonahydrate, $Fe(NO_3)_3{\cdot}9H_2O$ is shown in Fig. 4. It is shown that total mass loss of 83.1 wt% was determined up to 390 °C. The first DTG peak indicates the removal of physisorbed water and water of crystallization. The second peak refers to the decomposition of ferric hydroxide and formation of ferric oxide. Figure 5 shows the FT-IR spectrum of the zinc

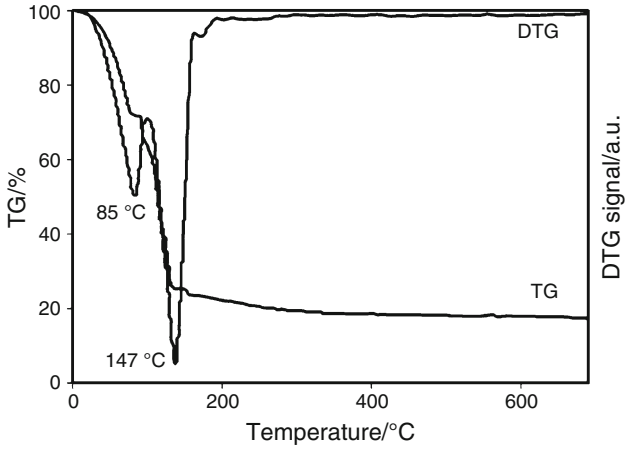

Fig. 1 Thermal curves of zinc acetate monohydrate as a precursor in sol–gel preparation of zinc ferrite nanoparticles

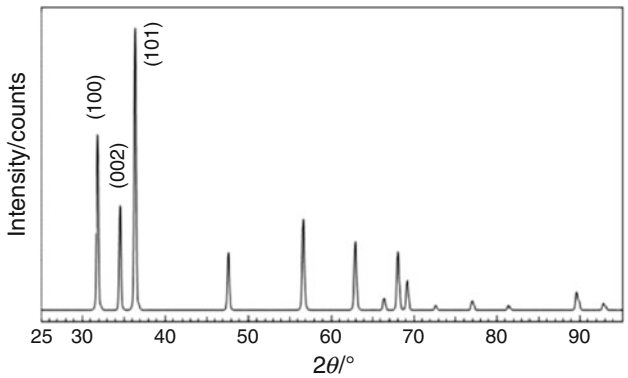

Fig. 2 XRD pattern of pure zinc oxide nanoparticle prepared by sol–gel method

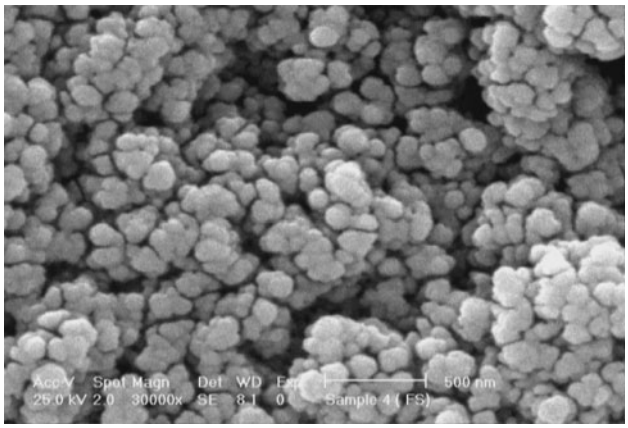

Fig. 3 Scanning electron microscopy micrograph of pure zinc oxide nanoparticle prepared by sol–gel method

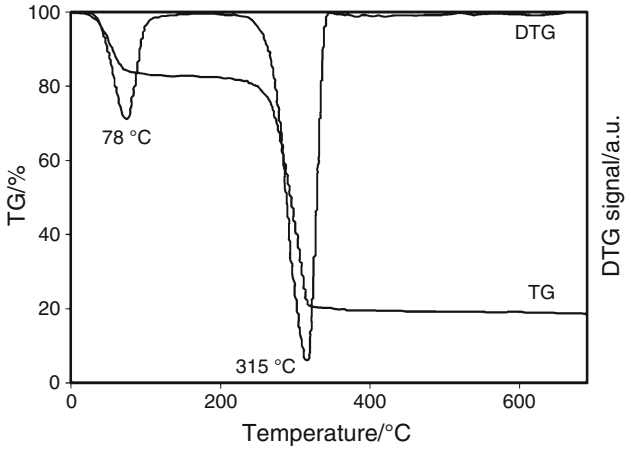

Fig. 4 Thermal curves of the Iron nitrate nonahydrate as a precursor in sol–gel preparation of zinc ferrite nanoparticles

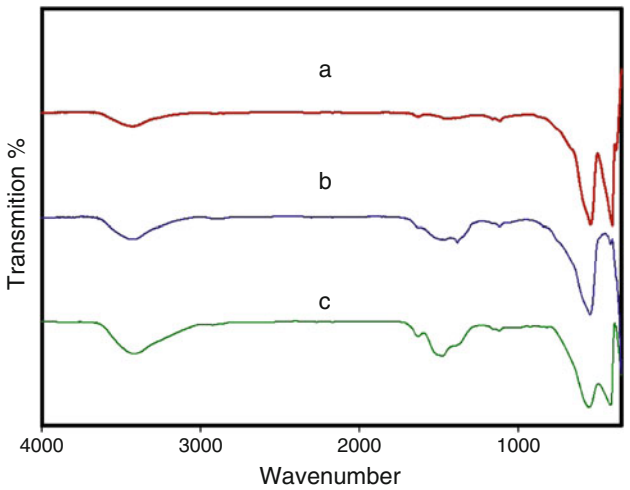

Fig. 5 FT-IR spectrum of the zinc ferrite nanoparticle prepared by sol–gel process using zinc acetate monohydrate and iron nitrate nonahydrate as precursors annealed at **a** 550 °C, **b** 450 °C, **c** 350 °C

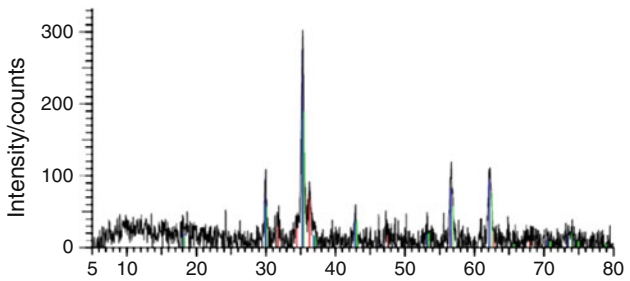

Fig. 6 XRD pattern zinc ferrite nanoparticle prepared by sol–gel process using zinc acetate monohydrate and iron nitrate nonahydrate as precursors

ferrite nanocomposite particles annealed at 450 °C. The broad band centered at 3430 cm^{-1} is due to the –OH groups. The peak at 735 cm^{-1} is a characteristic absorption of Fe–O. The peak at 548 cm^{-1} is a characteristic absorption of ZnO and the IR data are in consistence with the reported values [7, 8, 22, 30–32]. Figure 6 shows the XRD patterns of the zinc ferrite sample calcined at 450 °C.

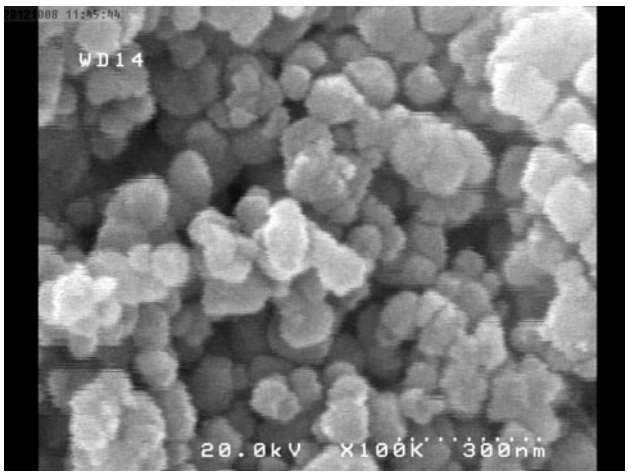

Fig. 7 FESEM micrograph of zinc ferrite nanoparticle prepared by sol–gel process using zinc acetate monohydrate and iron nitrate nonahydrate as precursors

As shown in Fig. 2, characteristic peaks of $ZnFe_2O_4$ are identified in the patterns of the sample which calcined at 350 °C. Figure 2 shows the X-ray patterns of the samples after calcination of the product obtained from 1 mmol of zinc acetate monohydrate, $Zn(C_2H_3O_2)_2{\cdot}H_2O$ and 2 mmol of iron nitrate nonahydrate, $Fe(NO_3)_3{\cdot}9H_2O$. The peaks at 29.95, 35.22, 36.73, 42.89, 56.53, and 62.34° can be readily ascribed to the characteristic peaks of the cubic phase of $ZnFe_2O_4$ (spinel ferrite) [33–41]. Reaction in the formation of $ZnFe_2O_4$ during the calcination process is presented as follows:

$$Zn(OH)_2 + 2Fe(OH)_3 \longrightarrow ZnFe_2O_4 + 4H_2O$$

FESEM micrograph (Fig. 7) of the zinc ferrite nanocomposite indicate that particles were uniformly spherical nanograins of $ZnFe_2O_4$ spinel [33].

Acknowledgements The authors wish to thank the University of Isfahan for financially supporting this work.

References

1. Gedam NN, Padole PR, Rithe SK, Chaudhari GN. Ammonia gas sensor based on a spinel semiconductor, $Co_{0.8}Ni_{0.2}Fe_2O_4$ nanomaterial. J Sol–Gel Sci Technol. 2009;50:296–300.
2. Kamble RC, Shaikh PA, Kamble SS, Kolekar YD. Effect of cobalt substitution on structural, magnetic and electric properties of nickel ferrite. J Alloys Compd. 2009;478:599–603.
3. Sedlar M, Pust L. Preparation of cobalt doped nickel ferrite thin films on optical fibres by dip-coating technique. Ceram Int. 1995;21:21–7.
4. Chen Z, Gao L. Synthesis and magnetic properties of $CoFe_2O_4$ nanoparticles by using PEG as surfactant additive. Mater Sci Eng B. 2007;141:82–6.
5. Sawant SY, Verenkar VMS, Mojumdar SC. Preparation, thermal, XRD, chemical and FTIR spectral analysis of $NiMn_2O_4$ nanoparticles and respective precursor. J Therm Anal Calorim. 2007;90:669–72.
6. More A, Verenkar VMS, Mojumdar SC. Nickel ferrite nanoparticles synthesis from novel fumarato-hydrazinate precursor. J Therm Anal Calorim. 2008;94(1):63–7.
7. Gonsalves LR, Verenkar VMS, Mojumdar SC. Preparation and characterization of $Co_{0.5}Zn_{0.5}Fe_2(C_4H_2O_4)3.6N_2H_4$: a precursor to prepare $Co_{0.5}Zn_{0.5}Fe_2O_4$ nanoparticles. J Therm Anal Calorim. 2009;96(1):53–7.
8. Gonsalves LR, Verenkar VMS, Mojumdar SC. Synthesis of cobalt nickel ferrite nanoparticles via autocatalytic decomposition of the precursor. J Therm Anal Calorim. 2010;100:789–92.
9. Porob RA, Khan SZ, Mojumdar SC, Verenkar VMS. Synthesis, TG, DSC and infrared spectral study of $NiMn_2(C_4H_4O_4)_{3.6}N_2H_4$: a precursor for $NiMn_2O_4$ nano-particles. J Therm Anal Calorim. 2006;86(3):605–8.
10. Habibi MH, Askari E. Thermal and structural studies of zinc zirconate nanoscale composite derived from sol–gel process: the effects of heat-treatment on properties. J Therm Anal Calorim. 2012; doi:10.1007/s10973-012-2205-x.
11. Habibi MH, Askari E. The effect of operational parameters on the photocatalytic degradation of CI reactive yellow 86 textile dye using manganese zinc oxide nanocomposite thin films. J Adv Oxid Technol. 2011;14:190–5.
12. Wu JJ, Tseng CH. Photocatalytic properties of nc-Au/ZnO nanorod composites. Appl Catal B. 2006;66:51–7.
13. Habibi MH, Mikhak M. Synthesis of nanocrystalline zinc titanate ecandrewsite by Sol–Gel: optimization of heat treatment condition for red shift sensitization. Curr Nanosci. 2010;7:603–7.
14. Iliev V, Tomova D, Todorovska R, Oliver D, Petrov L, Todorovsky D, Unova-Bujnova M. Photocatalytic activity of Ag/ZnO heterostructure nanocatalyst: correlation between structure and property. Appl Catal A. 2006;313:115–20.
15. Habibi MH, Sheibani R. Preparation and characterization of nanocomposite ZnO–Ag thin film containing nano-sized Ag particles: influence of preheating, annealing temperature and silver content on characteristics. J Sol–Gel Sci Technol. 2010;54:195–202.
16. Habibi MH, Sheibani R. Removal of 2-mercaptobenzoxazole from water as model of odorous mercaptan compounds by a heterogenous photocatalytic process using Ag–ZnO nanocomposite coated thin film on glass plate. Bull Environ Contam Toxicol. 2010;85:589–92.
17. Habibi MH, Sheibani R. Photocatalytic oxidation of four model mercaptans from aquatic environment using Ag–ZnO nanocomposite thin film for odor control. J Adv Oxid Technol. 2010;13:192–9.
18. Habibi MH, Sheibani R. Preparation and characterization of nanocomposite ZnO–Ag thin film containing nano-sized Ag particles: influence of preheating, annealing temperature and silver content on characteristics. J Sol–Gel Sci Technol. 2010;54:195–202.
19. Habibi MH, Askari E. Synthesis of nanocrystalline zinc manganese oxide by thermal decomposition of new dinuclear manganese(III) precursors. J Therm Anal Calorim. 2012; doi:10.1007/s10973-012-2460-x.
20. Habibi MH, Shojaee E, Yamane Y, Suzuki T. Synthesis, spectroscopic studies, crystal structure and electrochemical properties of new cobalt(III) complex derived from 2-aminophenol and 4-(dimethylamino) cinnamaldehyde: nano-sized complex thin film formation via surface layer-by-layer chemical deposition method. J Inorg Organomet Polym. 2012;22:190–5.
21. Habibi MH, Mikhak M. Titania/zinc oxide nanocomposite coatings on glass or quartz substrate for photocatalytic degradation of Direct Blue 71. Appl Surf Sci. 2010; doi:10.1016/j.apsusc.2012.03.042.
22. Gonsalves LR, Mojumdar SC, Verenkar VMS. Synthesis and characterization of ultrafine spinel ferrite obtained by precursor combustion technique. J Therm Anal Calorim. 2012;108:859–63.

23. Vital A, Angermann A, Dittmann R, Graule T, Topfer J. Highly sinter-active (Mg–Cu)–Zn ferrite nanoparticles prepared by flame spray synthesis. Acta Mater. 2007;55:1955–64.
24. Hua ZH, Chen RS, Li CL, Yang SG, Lu M, Gu XB, Du YW. $CoFe_2O_4$ nanowire arrays prepared by template-electrodeposition method and further oxidization. J Alloys Compd. 2007;427:199–203.
25. Thakur S, Katyal SC, Singh M. Structural and magnetic properties of nano nickel–zinc ferrite synthesized by reverse micelle technique. J Magn Magn Mater. 2009;321:1–7.
26. Maensiri S, Masingboon C, Boonchom B, Seraphin S. A simple route to synthesize nickel ferrite ($NiFe_2O_4$) nanoparticles using egg white. Scr Mater. 2007;56(9):797–800.
27. Jiang J. A facile method to the $Ni_{0.8}Co_{0.2}Fe_2O_4$ nanocrystalline via a refluxing route in ethylene glycol. Mater Lett. 2007;61:3239–42.
28. Gaur MS, Indolia AP. Thermally stimulated dielectric properties of polyvinylidenefluoride–zinc oxide nanocomposites. J Therm Anal Calorim. 2011;103:977–85.
29. Rishikeshi SN, Joshi S. Cu–ZnO nanocrystallites by aqueous thermolysis method: thermal and vibrational study. J Therm Anal Calorim. 2012;109:1473–9.
30. Lopez-Romero S, Leal SM. Fe_2O_3/ZnO composite particles prepared by a two step chemical soft method. Rev Mex Fıs. 2011;57(3):236–40.
31. Habibi MH, Kiani N. Preparation of single-phase α-Fe(III) oxide nanoparticles by thermal decomposition. Influence of the precursor on properties. J Therm Anal Calorim. 2012; doi:10.1007/s10973-012-2571-4.
32. Fu R, Wang W, Han R, Chen K. Preparation and characterization of γ-Fe_2O_3/ZnO composite particles Mater Lett. 2008;62:4066–4068.
33. Szczygiel I, Winiarska K. Low-temperature synthesis and characterization of the Mn–Zn ferrite. J Therm Anal Calorim. 2011;104:577–83.
34. Angus K, Thomas P, Guerbois J-P. Synthesis and characterisation of cobaltite and ferrite spinels using thermogravimetric analysis and X-ray crystallography. J Therm Anal Calorim. 2012;108:449–52.
35. Surzhikov AP, Lysenko EN, Vasendina EA, Sokolovskii AN, Vlasov VA. Thermogravimetric investigation of the effect of annealing conditions on the soft ferrite phase homogeneity. Therm Anal Calorim. 2011;104:613–7.
36. Surzhikov AP, Pritulov AM, Lysenko EN, Sokolovskii AN, Vlasov VA. Influence of solid-phase ferritization method on phase composition of lithium-zinc ferrites with various concentration of zinc. Therm Anal Calorim. 2012;109:63–7.
37. Carp O, Patron L, Pascu G, Mindru I, Stanica N. Thermal investigations of nickel–zinc ferrites formation from malate coordination compounds. Therm Anal Calorim. 2006;84:391–4.
38. Waqas H, Qureshi and AH. Low temperature sintering study of nanosized Mn–Zn ferrites synthesized by sol–gel auto combustion process. J Therm Anal Calorim. 2010;100:529-535.
39. Waqas H, Qureshi AH. Influence of pH on nanosized Mn–Zn ferrite synthesized by sol–gel auto combustion process. J Therm Anal Calorim. 2009;98:355–60.
40. Ichiyanagi Y, Uehashi T, Yamada S, Kanazawa Y, Yamada T. Thermal fluctuation and magnetization of Ni–Zn ferrite nanoparticles by particle size. J Therm Anal Calorim. 2005;81:541–4.
41. Xavier CS, Candeia RA, Bernardi MIB, Lima SJG, Longo E. Effect of the modifier ion on the properties of $MgFe_2O_4$ and $ZnFe_2O_4$ pigments. J Therm Anal Calorim. 2007;87:709–13.